

# Characterizing far from equilibrium states of the one-dimensional nonlinear Schrödinger equation

Abhik Kumar Saha<sup>1</sup> and Romain Dubessy<sup>2,\*</sup>

<sup>1</sup>*School of Physical Sciences, Indian Association for the Cultivation of Science, Jadavpur, Kolkata 700032, India*

<sup>2</sup>*Université Sorbonne Paris Nord, Laboratoire de Physique des Lasers,  
CNRS, UMR 7538, F-93430, Villetaneuse, France*

(Dated: October 19, 2022)

We use the mathematical toolbox of the inverse scattering transform to study quantitatively the number of solitons in a far from equilibrium one-dimensional system described by the defocusing nonlinear Schrödinger equation. We show that combining two simple criteria we are able to identify the localized eigenvalues of the Lax operator, corresponding to grey solitons and distinguish them from the continuous part of the spectrum, corresponding to plane-wave excitations. We apply this to the study of spatially periodic states and evidence the opening of multiple gaps in the spectrum. Our method can be applied in principle to all physical systems described by the defocusing nonlinear Schrödinger equation and allows to identify the solitons in numerical simulations.

## I. INTRODUCTION

The one-dimensional (1D) homogeneous non linear Schrödinger equation (1DNLSE):

$$i \frac{\partial \psi(z, t)}{\partial t} = \left( -\frac{1}{2} \frac{\partial^2}{\partial z^2} + g |\psi(z, t)|^2 \right) \psi(z, t), \quad (1)$$

where  $g$  quantifies the strength of the nonlinear term, written here in dimensionless form, is a very common model arising as a limiting case in the description of various physical phenomena, as for example: the propagation of monochromatic light in non linear optical fibers [1–4] or atomic vapors [5], ultra-cold atoms confined in very elongated traps [6–8], polariton superfluids [9] and the propagation of surface waves in deep water [10]. Several mathematical tools have been developed and successfully applied to study the solutions of Eq. (1), among which the inverse scattering transform (IST) that evidenced the existence of solitons [11–15], Whitham’s modulation theory that describes dispersive shock waves [16, 17], Lagrangian models [18–20] and numerical methods enabling the accurate propagation of initial conditions.

Thanks to the fine control of ultracold quasi 1D atomic gases it is possible to study experimentally the stability of solitons [21], soliton scattering on impurities [22], soliton creation by phase imprinting [7, 23] or head-on soliton collisions [24]. This has motivated numerous theoretical works to predict the soliton dynamics, following a phase-imprinting [25, 26], in the presence of an external trap [27] or an obstacle [28, 29] and to study finite temperature equilibrium states [30–33].

Equation (1) possesses many interesting properties that are related to its integrability and are well understood within the IST framework. In particular the IST introduces the Lax operator [14]:

$$\mathcal{L} = \frac{i}{2} \begin{pmatrix} \frac{\partial}{\partial z} & -\sqrt{g} \psi(z, t) \\ \sqrt{g} \psi(z, t)^* & -\frac{\partial}{\partial z} \end{pmatrix}, \quad (2)$$

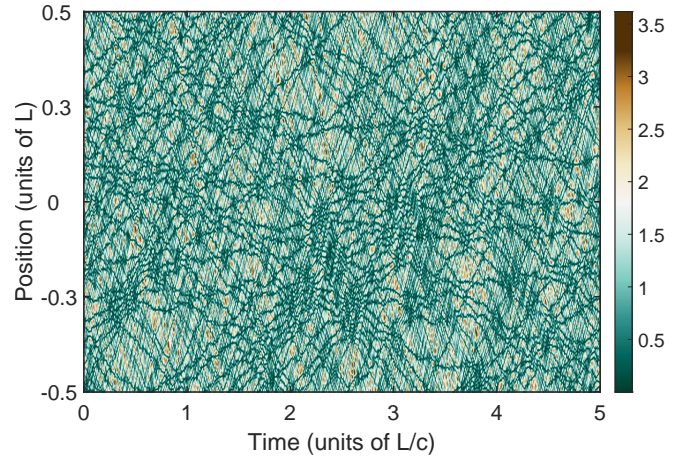


FIG. 1. (color online) Density map of a far from equilibrium state evolving according to the 1DNLSE, exhibiting large density fluctuations, with many propagating solitons. The quantity plotted is  $|\psi(z, t)|^2/N$ , normalized to the number of particles. We identify  $N_s = 122$  solitons propagating in this particular realization. See text for details on how the initial state is produced and solitons are detected.

that we write here for the  $g > 0$  de-focusing case. The operator defined by (2) is hermitian and importantly its (real) spectrum is time-invariant: therefore it can be used to classify and study the properties of a particular realization of the field  $\psi$ . For infinite systems with well defined asymptotic boundary conditions the IST predicts that the spectrum of the Lax operator  $\mathcal{L}v = \zeta v$ , that we will call the *Lax spectrum* hereafter, is made of two continuous branches separated by a gap, in which discrete eigenvalues may exist [11]. These discrete eigenvalues are directly related to the presence of solitons propagating in the system, are proportional to their velocity and the gap size is set by the speed of sound  $c \simeq \sqrt{gn_0}$ , where  $n_0$  is the background density.

The problem we address in this work is the following: how to characterize far from equilibrium states evol-

\* romain.dubessy@univ-paris13.fr

ing according to the 1DNLSE? To be more precise we aim at studying states with complex features, involving many solitons simultaneously propagating, as for example shown in the density map of Fig. 1. This task is in general difficult and may require sophisticated algorithms [34]. We will not address all the mathematical subtleties of the IST [14, 35] but rather consider practical details for potentially useful cases.

Importantly we will work with a finite size system, with periodic boundary conditions, which simplifies the numerical simulation of Eq. (1). We will show that the Lax spectrum is an efficient and convenient way of characterizing the far from equilibrium states and in particular enables to count precisely the number of solitons and determine their velocities. The main difficulty will be to identify which eigenvalues correspond to solitons as all eigenvalues are real for the defocusing case. Such an approach is simpler in the focusing case ( $g < 0$ ) and has already found applications [10], as in this regime the eigenvalues corresponding to solitons have an imaginary part, which separates them clearly from the background.

We note that several results are available concerning the 1DNLSE with periodic boundary conditions: the stationary states are known [36] and a specific form of the IST has been developed to take into account the periodicity [35, 37–39]. However we have found that the method of Ref. [38] leads to unstable numerical schemes for the large nonlinearities considered in the present work and therefore we rely on the study of the generic Lax operator of Eq. (2).

In this work we introduce two complementary measures allowing to properly identify the localized eigenstates in the Lax spectrum, based on the eigenvalue density and on the localization of the associated eigenvectors. We also study the Lax spectrum associated to states with spatial periodicity and evidence that its structure is deeply modified. This can be understood by mapping the Lax eigenvalue equation on a Schrodinger equation for a fictitious particle moving in a periodic potential. Our findings can be used to recover the properties of solitons in far from equilibrium 1D systems both in simulations and in experiments.

The paper is organized as follows: in section II, we recall basic properties of operator (2) for simple solutions of Eq. (1), then in section III, we study the Lax spectrum of the state shown in Fig. 1 and introduce tools to classify the eigenstates, in section IV we show that states with spatial periodicity exhibit Lax spectrum with multiple gaps and discuss their relevance for experiments. Finally we discuss our results and conclude in section V.

## II. PROPERTIES OF THE LAX OPERATOR

As mentioned above we use periodic boundary conditions, such that  $\psi(z, t) = \psi(z + L, t)$  with  $L$  the size of the system and we normalize the field to a total number of particles:  $N = \int_{-L/2}^{L/2} dz |\psi(z, t)|^2$ . In the limit

of a very large system  $L \rightarrow \infty$  keeping a fixed average density  $N/L = n_0$ , Eq. (1) has a well known family of solutions corresponding to the propagation of a single soliton [8, 40]:

$$\psi_1(z, t) = \sqrt{n_1} e^{i(k_0 z - \omega t)} (B \tanh(B\sqrt{gn_1}[z - \bar{z}(t)]) + iA), \quad (3)$$

where  $n_1 \gtrsim n_0$  is the background density,  $B = \cos \phi$  and  $A = \sin \phi$  are given by the soliton angle  $\phi \in [-\pi/2, \pi/2]$  that controls its depth and velocity  $v \equiv \dot{\bar{z}}(t)$ . The solution defined by Eq. (3) exists provided that the frequency  $\omega = gn_1 + k_0^2/2$  and  $v = k_0 + A\sqrt{gn_1}$ , where  $k_0$  is fixed by the periodic boundary conditions:

$$e^{ik_0 L} = \frac{iA - B \tanh(B\sqrt{gn_1}L/2)}{iA + B \tanh(B\sqrt{gn_1}L/2)}.$$

Here it is necessary to include this  $k_0$  contribution because of the periodic boundary conditions: the phase jump associated to the presence of a single soliton has to be compensated by an opposite global phase gradient. This also slightly modifies the relation between the velocity of the soliton and its angle with respect to the infinite size system. This constrain is obviously relaxed when considering an open system.

Equation (3) simplifies to the homogeneous ground-state solution  $|\psi_0| = \sqrt{n_0}$  for  $\phi \rightarrow \pm\pi/2$  and to the dark soliton solution, for which the density vanishes at the center of the soliton, when  $\phi = 0$ . Interestingly it is possible to compute the Lax spectrum analytically for this family of solutions: it is made of two continuous branches

$$\zeta_q^\pm = -\frac{k_0}{4} \pm \frac{\sqrt{gn_1 + q^2}}{2},$$

associated to de-localized quasi plane-wave eigenstates

$$v_q^\pm \propto e^{\pm i q z} \begin{pmatrix} e^{i \frac{k_0 z - \omega t}{2}} \left[ i \frac{k_0 + 4\zeta_q^\pm \mp 2q}{2\sqrt{gn_1}} + \frac{\psi_1(z, t)}{\sqrt{n_1} e^{i(k_0 z - \omega t)}} \right] \\ e^{-i \frac{k_0 z - \omega t}{2}} \left[ i \frac{k_0 + 4\zeta_q^\pm \pm 2q}{2\sqrt{gn_1}} - \frac{\psi_1(z, t)^*}{\sqrt{n_1} e^{-i(k_0 z - \omega t)}} \right] \end{pmatrix}$$

and a single discrete eigenvalue

$$\zeta_0 = -\frac{k_0}{4} - \frac{\sqrt{gn_1}}{2} \sin \phi,$$

corresponding to a localized state

$$v_0 \propto \text{sech}(B\sqrt{gn_1}[z - \bar{z}(t)]) \begin{pmatrix} e^{i \frac{k_0 z - \omega t}{2}} \\ -e^{-i \frac{k_0 z - \omega t}{2}} \end{pmatrix}.$$

Here we use the term quasi plane wave to describe the de-localized eigenvalues because of the  $e^{\pm i q z}$  dependence,  $q \in 2\pi/L \times \mathbb{Z}$  being the 1D wave-vector. Interestingly the localized state is peaked around the position of the density dip associated to the soliton.

As mentioned above, the eigenvalues of the Lax spectrum are time invariant, while the eigenvectors explicitly depend on time. Moreover it is easy to verify that the

discrete eigenvalue lies in the gap between the upper  $\zeta_q^+$  and lower  $\zeta_q^-$  branches, that are doubly degenerate as  $\zeta_q^\pm = \zeta_{-q}^\pm$ . This is in fact a consequence of the symmetry of the Lax operator.

Indeed it is easy to verify that

$$\sigma \mathcal{L} \sigma = \mathcal{L}^*, \text{ where } \sigma = \begin{pmatrix} 0 & 1 \\ 1 & 0 \end{pmatrix},$$

such that if  $v$  is an eigenvector with eigenvalue  $\zeta$  then  $v' = \sigma v^*$  is also an eigenvector with the same eigenvalue. Therefore one can expect that most of the eigenvalues are doubly degenerate and that non degenerate eigenvalues satisfy  $v' \propto v$ .

Applying the unitary transform:

$$U = \begin{pmatrix} e^{i\phi(z)/2} & 0 \\ 0 & e^{-i\phi(z)/2} \end{pmatrix}$$

to  $\mathcal{L}$  results in:

$$\mathcal{L}' = U^\dagger \mathcal{L} U = \frac{i}{2} \begin{pmatrix} \frac{\partial}{\partial z} & -\sqrt{g}\psi e^{-i\phi} \\ \sqrt{g}\psi^* e^{i\phi} & -\frac{\partial}{\partial z} \end{pmatrix} - \frac{1}{4} \frac{\partial \phi}{\partial z} \begin{pmatrix} 1 & 0 \\ 0 & 1 \end{pmatrix},$$

which results immediately in the fact that a boost of momentum  $q$  applied to  $\psi \rightarrow \psi e^{iqz}$  simply shifts globally all the Lax spectrum by  $-q/4$ . This explains why the eigenvalues of the single soliton state are all shifted by  $-k_0/4$ . It shows also that the gap boundaries need not to be symmetric with respect to zero and consequently that the total current in a ring geometry is encoded in the shift of the Lax spectrum. In section III, we will introduce a method to detect faithfully the gap boundaries for arbitrary states.

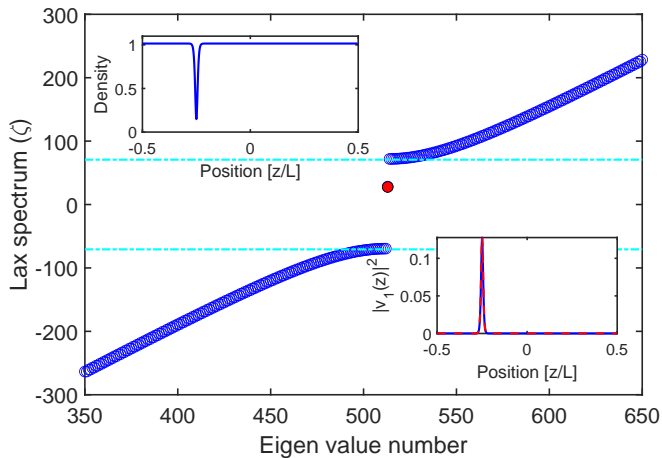


FIG. 2. (color online) Lax spectrum for a single grey soliton state: open blue circles indicate continuous branches of the spectrum, the single filled red circle is the discrete eigenvalue associated to a localized eigenstate and the two horizontal dashed cyan lines correspond to the gap boundaries at  $-k_0/4 \pm \sqrt{gn_1}/2$ . Upper inset: density of the single grey soliton state evidencing the density dip. Lower inset: square modulus of the eigenvector corresponding to the localized eigenvalue (blue solid line) compared to the analytical prediction (red dashed line).

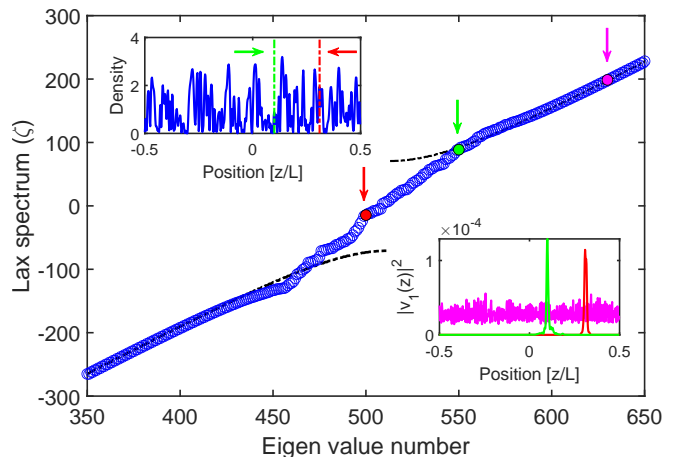


FIG. 3. (color online) Lax spectrum as a function of eigenvalue number for the out of equilibrium state of figure 1 (open blue circles). The two black dashed-dotted lines indicate for comparison the Lax spectrum of the ground state. Upper inset: initial density profile. Lower inset: square modulus of three eigenvectors (solid red, green and magenta curves) corresponding to three particular eigenvalues identified by the arrows and the filled circles (red, green, magenta) in the main panel. The magenta curve is magnified by a factor  $\times 15$ .

Although these formulas are exact only in the limit  $L \rightarrow \infty$  they provide a very good approximation for finite size systems provided that the healing length  $\xi \simeq 1/\sqrt{2gN/L}$  is much smaller than  $L$ . Figure 2 shows the Lax spectrum for a single soliton state as defined by Eq. (3), evidencing the discrete, isolated, eigenvalue inside the gap and showing the agreement with analytical formula for the localized eigenstate. The fact that simple and quantitative results can be obtained at the moderate cost of the diagonalization of a relatively simple operator is promising for the study of arbitrary complex states. However, the simulation of Eq. (1) implies a discrete representation which introduces two difficulties: on the one hand the discretization of the differential operator (2) must be done carefully to avoid the apparition of spurious eigenvalues, see Appendix B, and, on the other hand, the notion of continuous branch in the spectrum becomes ill defined as by essence all eigenvalues are discrete for a finite size operator. We will discuss strategies to overcome this latter difficulty in the next section.

### III. LAX SPECTRUM OF FAR FROM EQUILIBRIUM STATES

Figure 3 shows the Lax spectrum associated to the state of Fig. 1. One can immediately see that the gap is not visible anymore and that the eigenvalues seem to be almost uniformly distributed. This can be interpreted as the fact that there are many solitons propagating, as can be seen in Fig. 1, such that the gap is filled with discrete eigenvalues. Such interpretation is supported by

the fact that some eigenvalues are associated to localized eigenvectors whereas other are still delocalized, see the lower inset of Fig. 3. Based on the analytical results of section II, it is natural to identify a localized eigenvector to a soliton propagating at a well defined velocity and localized at the position of the peak of the eigenvector modulus. We note that it is not evident to count the number of soliton by looking at the initial density profile (upper inset of Fig. 3) or the time evolution in the density map of Fig. 1.

In order to analyze more quantitatively the Lax spectrum we introduce now two new tools. First we consider the distance between adjacent eigenvalues, that we define as follows: given a discrete set of eigenvalues  $\{\zeta_i\}$  the local distance around eigenvalue  $\zeta_i$  is  $\mathcal{D}(\zeta_i) = \zeta_{i+1} - \zeta_{i-1}$ . With this definition  $\mathcal{D}(\zeta)$  can be seen as the inverse of the local density of eigenvalues. It is instructive to look at this quantity for the homogeneous ground-state for which the Lax spectrum is made of two doubly degenerate continuous branches. It is easy to compute the distance in that case:  $\mathcal{D}(\zeta_i) \simeq \delta q \sqrt{4\zeta_i^2 - gn_0/4|\zeta_i|}$ , for  $|\zeta_i| \geq \sqrt{gn_0}/2$ , i.e. outside the gap, and where  $\delta q$  is the grid spacing in momentum space:  $\delta q = 2\pi/L$ . Therefore  $\mathcal{D}(\zeta)$  is vanishing at the two gap edges and approaches  $\pi/L$  for large eigenvalues.

Figure 4a) shows this distance as a function of the eigenvalue, for both the groundstate (dashed-dotted black curve) and for the out of equilibrium state (open blue circles). In both cases, the distance far from the gap converges to the predicted value of  $\pi/L$  however the variations of the distance in the vicinity of the gap edges are not trivial to interpret and this criterion alone is not sufficient to distinguish discrete eigenvalues from continuous branches, in this case. However one can already guess that the gap in the Lax spectrum is larger for the excited state than for the groundstate with the same number of particles.

To obtain a better criterion, we study the localization of the eigenvectors associated to each eigenvalues. This can be simply estimated by looking at the maximum value of the square modulus of the eigenvector, provided that the eigenvectors are normalized. Indeed we expect this maximum to be roughly proportional to the inverse of the localization size. Similarly one can also consider the eigenvectors in Fourier space, where in this case the maximum value of the square modulus will be large for de-localized states.

More precisely, given the eigenvector  $v(z, t) = (v_1(z, t), v_2(z, t))^T$  associated to eigenvalue  $\zeta$ , we compute the value:

$$\mathcal{M}(\zeta, t) = L \frac{\sum_{i=1,2} \max_z |v_i(z, t)|^2}{\sum_{i=1,2} \max_k |\hat{v}_i(k, t)|^2},$$

where  $z \in [-L/2, L/2]$ ,  $\hat{v}_i(k)$  is the Fourier transform of  $v_i(z, t)$ , with respect to the space coordinate  $z$ . It is again instructive to study limiting cases. For the groundstate we expect only de-localized plane-wave eigenstates, with

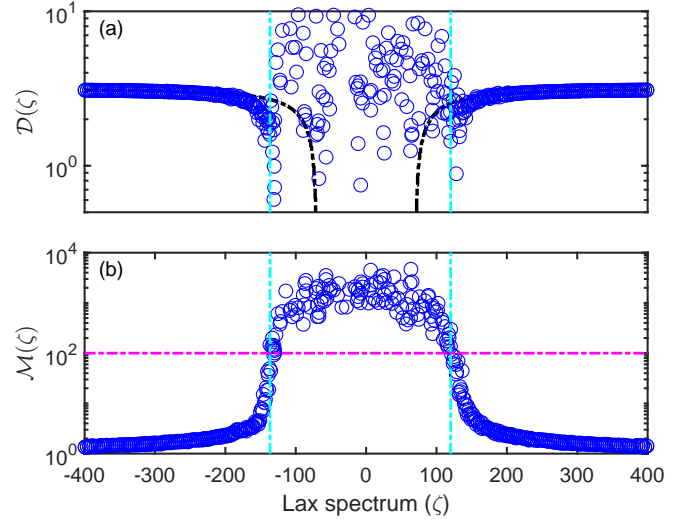


FIG. 4. (color online) a) Distance between adjacent eigenvalues as a function of the eigenvalue for the Lax spectrum of Fig. 3 (open blue circles) and for the ground state (dashed-dotted black curve), in log-linear scale. The continuous parts of the spectrum appear as regularly distributed eigenvalues while discrete eigenvalues are irregularly distributed. The density of eigenvalues increases at the gap edges. b) Localization measure as a function of eigenvalue for the Lax spectrum of Fig. 3 (open blue circles), in log-linear scale. The vertical dashed-dotted cyan lines indicate the main gap in the Lax spectrum. The dashed-dotted horizontal magenta line correspond to  $\mathcal{M}_c = 100$ . The discrete eigenvalues appear clearly as localized eigenstates. See text for details.

uniform density and therefore  $\mathcal{M} = 1$  for all eigenvalues. We may expect that the most localized eigenstate occurs for a dark soliton for which it is straightforward to compute that  $\mathcal{M} \simeq gN/\pi^2$ .

Figure 4b) shows the value  $\mathcal{M}(\zeta, t)$  for the out of equilibrium state, evidencing that the eigenvalues can be classified as localized or de-localized according to this criterion. To distinguish localized eigenvectors from de-localized states we use the phenomenological criterion  $\mathcal{M}_c = 100$ : above this threshold we consider that the eigenvalues correspond to localized propagating solitons.

Although there is a clear correlation with the largest  $\mathcal{M}$  values found near the gap center, where we expect the deepest and more localized solitons, we observe some fluctuations in the distribution of  $\mathcal{M}$  values. At first it may seem surprising that there is no simple relation between the eigenvalue  $\zeta$  in the gap and its  $\mathcal{M}$  value, considering that slower solitons should give more localized states, according to Eq. (3). However one has to remember that if the Lax eigenvalues  $\zeta$  are time-independent, the Lax eigenvectors  $v$  are not and that there is no reason that their shape remains fixed during the evolution. In particular consider what happens during a collision between two solitons: it is known that they cross each other without changing their properties which is a consequence of integrability [11]. However, during the crossing the width



of the density dip due to the two solitons is larger, offering more space for the eigenstates to expand and therefore lowering their  $\mathcal{M}$  values, see Appendix C. This suggests that to obtain a faithful estimation of the gap one has to sample the state at different times throughout the evolution and take for each eigenvalue the largest of the  $\mathcal{M}$  values. However we have found that for typical far from equilibrium states as the one of figure 1, the computation of  $\mathcal{M}$  values from a single realization is sufficient to identify the gap.

#### IV. LAX SPECTRA WITH MULTIPLE CONTINUOUS BRANCHES

In this section we show that for some initial states the Lax spectrum can exhibit multiple continuous branches, or, put differently, that it is possible to have delocalized states associated to eigenvalues inside the gap. This is expected from the study of the IST with periodic boundary conditions [35], but we provide a physically intuitive explanation based on a mapping of the Lax eigenvalue problem to a linear Schrödinger equation [41].

The eigenvalue equation  $\mathcal{L}v = \zeta v$  involving operator (2) can be written explicitly:

$$\begin{aligned} \left( \frac{\partial}{\partial z} + 2i\zeta \right) v_1 &= \sqrt{g}\psi v_2, \\ \left( \frac{\partial}{\partial z} - 2i\zeta \right) v_2 &= \sqrt{g}\psi^* v_1, \end{aligned}$$

and after a straightforward manipulation, introducing  $v_{\pm} = v_1 \pm v_2$  and  $\psi = \text{Re}\psi + i\text{Im}\psi$ , one obtains:

$$\begin{aligned} 4\zeta^2 v_+ &= \left( -\frac{\partial^2}{\partial z^2} + g|\psi|^2 + \sqrt{g}\frac{\partial \text{Re}\psi}{\partial z} \right) v_+ - i\sqrt{g}\frac{\partial \text{Im}\psi}{\partial z} v_-, \\ 4\zeta^2 v_- &= \left( -\frac{\partial^2}{\partial z^2} + g|\psi|^2 - \sqrt{g}\frac{\partial \text{Re}\psi}{\partial z} \right) v_- + i\sqrt{g}\frac{\partial \text{Im}\psi}{\partial z} v_+, \end{aligned}$$

which is formally equivalent to the Schrödinger equation for a spin-1/2 particle:

$$E\Psi = \left( -\frac{1}{2}\frac{\partial^2}{\partial z^2} + \frac{g|\psi|^2}{2} + \frac{\sqrt{g}}{2}\frac{\partial \text{Re}\psi}{\partial z}\sigma_z + \frac{\sqrt{g}}{2}\frac{\partial \text{Im}\psi}{\partial z}\sigma_y \right) \Psi,$$

where  $E \equiv 2\zeta^2$ ,  $\Psi \equiv (v_+, v_-)^T$  and  $\sigma_{x,y,z}$  are the Pauli matrices. Therefore the Lax spectrum of the 1DNLS (1) can be obtained by finding the positive spectrum of a Schrödinger equation, which in general consists in a continuous spectrum of de-localized states and localized bound states.

To further discuss this analogy it is convenient to consider the case of a real valued field  $\psi$ , which gives a simpler equation:

$$Ev_{\pm} = \left( -\frac{1}{2}\frac{\partial^2}{\partial z^2} + V_{\pm}(z) \right) v_{\pm},$$

where the effective potential is:

$$V_{\pm}(z) = \frac{g}{2}|\psi|^2 \mp \frac{\sqrt{g}}{2}\frac{\partial \psi}{\partial z}.$$

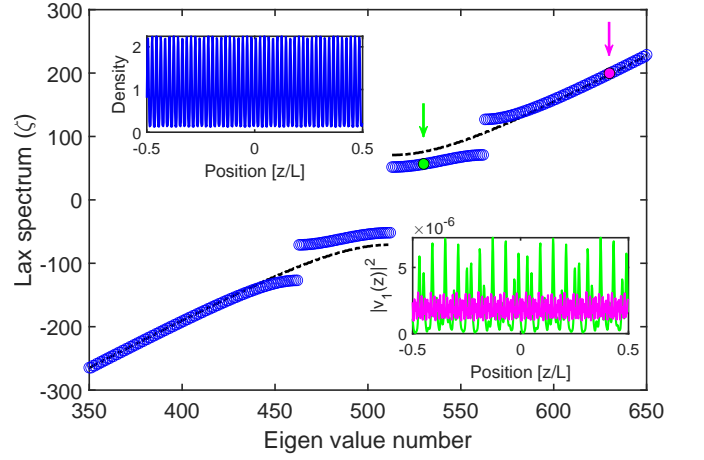


FIG. 5. (color online) Lax spectrum as a function of eigenvalue number for a highly periodic initial state (open blue circles). The two black dashed-dotted lines indicate for comparison the Lax spectrum of the ground state with the same parameters. Upper inset: initial density profile. Lower inset: square modulus of two eigenvectors (solid green and magenta curves) corresponding to two particular eigenvalues identified by the filled circles (green and magenta) in the main panel.

In this particular case one can expect that all eigenstates with energy  $E > \max V_{\pm}(z)$  are delocalized, which provides a direct estimation of the gap in the Lax spectrum, whereas bound-states may exist for lower energies.

Now, if  $\psi$  is periodic (in space),  $V_{\pm}(z) = V_{\pm}(z + \ell)$  is also periodic and using Bloch theorem, we may write the eigenvectors:  $v_{\pm}(z) = e^{iqz}u_{\pm}(z)$ , where the Bloch functions  $u_{\pm}(z) = u_{\pm}(z + \ell)$  are periodic and  $q \in [-\frac{\pi}{\ell}, \frac{\pi}{\ell}]$  is the pseudo-momentum, restricted to the first Brillouin zone. As both the potential and the Bloch functions are  $\ell$ -periodic, we may use a Fourier series expansion:

$$V_{\pm}(z) = \sum_n V_n e^{ik_n z} \text{ and } u_{\pm}(z) = \sum_n u_n^{\pm} e^{ik_n z}.$$

where  $k_n = \frac{2\pi}{\ell}n$ , for  $n \in \mathbb{Z}$ , resulting in an infinite set of coupled equations:

$$\left( \frac{(q + k_n)^2}{2} + V_0 \right) u_n^{\pm} + \sum_{m \neq 0} V_m u_{n-m}^{\pm} = 2\zeta^2 u_n^{\pm}.$$

Therefore we obtain a set of equations similar to the one describing the movement of a particle in a periodic potential, as for electron in solids or atoms in optical-lattices. As is well known in this case the spectrum of the Schrödinger equation takes the form of a band structure in which, depending on the strength of the potential, the eigenstates are localized (in the tight binding regime) or de-localized (in the tunneling regime).

Interestingly this results in non trivial Lax spectra for states that have an initial periodicity where the underlying band structure appears as the opening of multiple gaps between continuous part of the spectrum. Figure 5 illustrates this behavior, where the lower inset emphasize

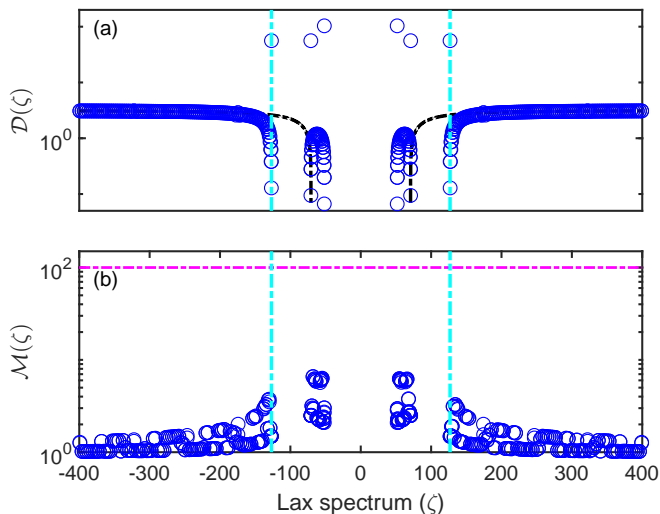


FIG. 6. (color online) a) Distance between adjacent eigenvalues as a function of the eigenvalue for the Lax spectrum of Fig. 5 (open blue circles) and for the ground state (dashed-dotted black curve), in log-linear scale. The distance is large for eigenvalues that are at the gap edges and the density of eigenvalues increases close to the edges. b) Localization measure as a function of eigenvalue for the Lax spectrum of Fig. 5 (open blue circles), in log-linear scale. All eigenvalues correspond to de-localized eigenstates. The vertical dashed-dotted cyan lines indicate the main gap in the Lax spectrum. The dashed-dotted horizontal magenta line correspond to  $\mathcal{M}_c = 100$ . See text for details.

that all eigenstates appear as delocalized. To the best of our knowledge it is the first report of such Lax spectrum structure with eigenvalues in the gap that are not solitons. Importantly the mapping to the Schrödinger equation and the use of the Bloch theorem proves that it is not a numerical artefact but a special feature of periodic states. Moreover we have found that this behavior exists also for states that are not purely real, but only  $\ell$  periodic, which represents a larger ensemble and may facilitate their creation in experiments (see section V for a discussion and appendix A for details).

Figure 6 confirms that indeed all eigenvalues of the Lax spectrum shown in Fig. 5 are delocalized, as their  $\mathcal{M}$  values remain low (well below 100). We note that in this case the distance  $\mathcal{D}(\zeta)$  is useful to find the gap edges: at each boundary the last (first) eigenvalue of the continuous spectrum is associated to a large  $\mathcal{D}$  value. From the distribution of  $\mathcal{D}(\zeta)$  we conclude that the Lax spectrum of this state consists in four continuous branches, separated by three gaps.

## V. DISCUSSION & CONCLUSION

In this work we have applied the analytical tools and methods developed in the IST framework to the study of far from equilibrium states exhibiting a rich dynamics. We have shown that despite the use of periodic bound-

ary conditions it was possible to efficiently find the Lax spectrum by diagonalizing an hermitian operator. Moreover we have studied how to identify properly the localized and de-localized states in a finite size system, using two simple criteria: the inverse local eigenvalue density  $\mathcal{D}(\zeta)$  and a measure of the localization of the eigenvectors  $\mathcal{M}(\zeta, t)$ . Using the mapping of the Lax spectrum problem onto a Schrödinger eigenvalue problem for a fictitious particle in an effective potential we have discussed the general structure of the Lax spectrum and have unveiled that exotic spectra may exist for states exhibiting spatial periodicity at a given time. We now discuss these results, their potential applications and the possibility to use this method to characterize experimental results.

First it is important to recall that the Lax spectrum is time-invariant and can be computed using the value of the field  $\psi(z, t)$  at any convenient time. More precisely the eigenvalues  $\zeta$  are time-independent while the eigenvectors evolve with time, following for example the trajectory of the solitons as shown in the insets of figures 2 and 3. If one is interested in determining the number of solitons *hidden* in a particular state the Lax spectrum is particularly useful: it is sufficient to compute it for the initial state, then determine the localized eigenvalues using the measures  $\mathcal{M}(\zeta, t)$  and  $\mathcal{D}(\zeta)$  to know precisely the number of solitons and their velocities. This can greatly simplify the task of identifying solitons by inspection of the density profile dynamics, which is almost impossible for very excited states, see for example Fig. 1.

One surprising result of our work is the possibility to find eigenvalues within the gap that do not correspond to solitons but to delocalized states. We have shown that this could be explained when the state  $\psi(z, t)$  is periodic in space by a mapping to an appropriate periodic Schrödinger equation. Although the existence of these eigenvalues seem to contradict the classification of Ref. [11], it is simply due to the different choice of boundary conditions, that allow in our work states that were not considered in the original IST framework. The state corresponding to the Lax spectrum of Fig. 5 is not a stationary solution of the 1DNLS but rather a time-periodic solution [35], with a rich dynamics. We have found that it belongs to a large family of states that can be generated by the initial condition:

$$\psi_2(z, t) = \sqrt{n_0}(1 + \epsilon \cos k_0 z), \quad (4)$$

where  $n_0$  is the background density,  $\epsilon$  is a perturbation amplitude and  $k = 2\pi/\ell$  defines the periodicity. Interestingly, we have observed that for  $k < 1/\xi$  the state defined by Eq. (4) corresponds to the propagation of degenerate groups of solitons, with the same velocity and a degeneracy given by the ratio  $L/\ell$ , while for  $k > 1/\xi$  the state exhibits a time-periodic behavior in its density pattern, with only delocalized eigenvalues.

Importantly, the states that we have studied in sections III and IV can be created starting from the ground-state by simple excitation protocols that can be readily implemented in experiments, in particular with ultra-cold

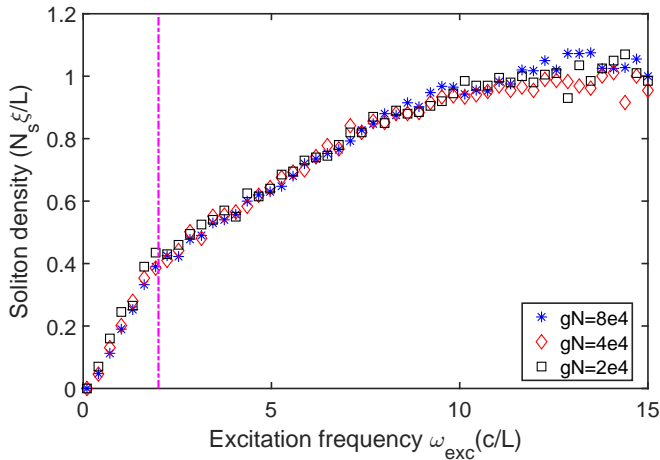


FIG. 7. (color online) Number of soliton per healing length  $N_s \times \xi/L$  as a function of the excitation frequency, for different values of the non-linear coefficient  $gN$ . For all curves, the number of soliton per healing length saturates around unity. The dashed-dotted vertical magenta line corresponds to  $\omega_{\text{exc}} = 2c/L$ . Because we vary the nonlinear coefficient  $gN$ , we adapt the threshold to detect localized eigenvalues  $\mathcal{M}_c$ . See text for details.

atoms, see Appendix A for details. For example, by modulating the position of a narrow Gaussian obstacle, see Eq. (A1), at a frequency  $\omega_{\text{exc}}$ , we are able to generate arbitrary numbers of solitons, as reported on Fig. 7. Our analysis protocol allows to extract for each simulation the number of solitons. We observe that the number of soliton per healing length increases with the excitation frequency, saturates at a value close to unity for large  $\omega_{\text{exc}}$  and follows a universal behavior, for different values of  $gN$ . Note that increasing  $gN$  increases  $c$  and reduces  $\xi$ , but also changes the maximum value of  $\mathcal{M}$ , corresponding to a dark soliton (see section III). Therefore we adapt our threshold definition by a simple rescaling:  $\mathcal{M}_c = 100 \times gN/(2 \times 10^4)$ , for each simulation. It must be noted that as the total amplitude of displacement of the barrier is set to  $L/2$  in our excitation protocol, one can expect that the motion of the barrier becomes resonant with soundwaves traveling at the speed of sound  $c$  when  $\omega_{\text{exc}} > 2c/L$ , thus explaining the change of slope at  $\omega_{\text{exc}} \simeq 2c/L$ .

However, at this stage it must be noted that the realization of a 1D system with periodic boundary conditions is not so common. The IST framework is valid only for homogeneous systems, a condition that may seem too stringent for experiments that rely in general on a trap. However it can be extended with little effort to the case of a 1D box potential [42], recently realized for ultra-cold atoms, using a mirror image method. Indeed, for any state, box boundary conditions on the interval  $[0, L]$  are mathematically equivalent to periodic boundary conditions for a system extended to the interval  $[-L, L]$  with an anti-symmetric initial state. It is therefore possible to extend our results to box boundary conditions: the box

will then appear as a pair of eigenvalues at  $\zeta = 0$  in the Lax spectrum.

Finally we note that it is necessary to have access to the full field  $\psi(z, t)$ , at a given time, to be able to compute the Lax spectrum. Unfortunately it is not sufficient to measure the state density  $|\psi(z, t)|^2$ . This suggests that to apply this analysis tool to an experiment one has to perform at least two measurements on the state: an interferometric measurement giving access to the phase and a direct measurement of the density. This work only consider states in the mean-field limit and therefore the simultaneous measurement of the density and the phase should not be affected by quantum noise. These measurements can be challenging for ultra-cold atom experiments but are readily implemented in other systems described by the 1DNLSE as light propagation in non-linear fibers, fluids of lights or polariton systems, taking advantage of standard detection schemes of quantum optics, based on interferometers.

To summarize we have revisited the notion of the Lax spectrum in a broader context than in the original work on the IST. Although this come at the cost of some ambiguities in the interpretation of the discretized spectrum we have shown that simple tools allowed to identify the structure of the Lax spectrum for arbitrary states. Given the simplicity and the efficiency of the process, requiring only the diagonalization of an hermitian matrix, we believe that it will find many applications in the study of out-of-equilibrium states in the 1DNLSE, including studies with large ensembles of solitons. Moreover we think that this tool is specially appropriate to study how additional external potential terms entering in Eq. (1) break the integrability, which will result in a time dependent Lax spectrum, similarly to what has been observed in [10]. Finally it opens the way to study quantitatively the probability density of finding solitons with given velocity which is relevant to the study of one dimensional soliton turbulence and thermal equilibrium properties.

## ACKNOWLEDGMENTS

RD thanks Maxim Olshanii for introducing him to the inverse scattering transform method and for many inspiring discussions. LPL is UMR 7538 of CNRS and Sorbonne Paris Nord University.

## Appendix A: Methods

We provide here details on the numerical methods we use to study the 1DNLSE. To numerically solve Eq. (1), we use a spectral method relying on fast Fourier transforms to evaluate exactly the kinetic energy term [43], with a regular grid of  $N_z = 512$  points and a dimensionless nonlinear parameter  $gN = 2 \times 10^4$ , well within the mean field regime [44]. The grid introduces a natural cut-off for the wavevectors at  $k_{\text{max}} = \pi N_z/L$  and

to avoid aliasing in the computation of non-linear terms we use a projector onto the low  $k$  region:  $|k| < k_{\text{cut}} = 2k_{\text{max}}/3$  [45]. The integration in time is carried on using a standard fourth-order adaptive Runge-Kutta scheme.

The groundstate of Eq. (1) corresponds to a flat density profile:  $\psi_0 = \sqrt{n_0}$ , where  $n_0 = N/L$ , and the bare chemical potential  $\mu_0 = gn_0$  is the relevant energy scale, that fixes the healing length  $\xi = 1/\sqrt{2\mu_0}$  and the speed of sound  $c = \sqrt{\mu_0}$ .

To drive the system to out-of-equilibrium states we use two excitation protocols: (a) stirring with a Gaussian potential which is oscillating back and forth along the axial dimension of the condensate [46–50] and (b) by modulating the height of a periodic potential.

To implement the stirring protocol, we add to Eq. (1) the excitation potential in the form of a moving gaussian obstacle:

$$V_{\text{stirr}}(t, z) = V_b(t) \exp[-(z - z_c(t))^2/\sigma^2], \quad (\text{A1})$$

where  $V_b(t)$  is the time-dependent barrier height,  $\sigma = 4\xi$  is the width of the barrier and  $z_c(t) = \delta z \cos(\omega_{\text{exc}} t)$  is the position of the barrier. The amplitude of the motion is set to  $\delta z = L/4$ , the barrier is turned on in a time  $t_{\text{on}} = L/c$ , kept at its maximum value  $V_0 = \mu_0$  for  $T_{\text{exc}} = 8 \times L/c$  and turned off in a time  $t_{\text{off}} = L/c$ .  $V_0$  is chosen such that the density is nearly completely depleted at the peak of the barrier which facilitates the creation of solitons, while  $t_{\text{on}}$  and  $t_{\text{off}}$  are slow enough to prevent the creation of excitations if the barrier is not moving (i.e. for  $\omega_{\text{exc}} = 0$  or  $\delta z = 0$ ). We then vary  $\omega_{\text{exc}}$  to control the amount of excitation created in the final state. For example the state of Fig. 1 was generated with  $\omega_{\text{exc}} = 4.5 \times c/L$ .

For the modulation protocol, we use an excitation potential of the form

$$V_{\text{exc}}(t, z) = V_b(t) \frac{1 + \sin(k_{\text{exc}} z)}{2}, \quad (\text{A2})$$

where  $V_b(t) = V_1 \times (1 - \cos(\omega_{\text{exc}} t))/2$  is now a sinusoidal modulation and  $k_{\text{exc}} = 2\pi M/L$ ,  $M \in \mathbb{N}^*$  being the number of minima (or maxima) in the potential. We apply this potential for a total time  $T_{\text{exc}} = 5 \times 2\pi/\omega_{\text{exc}}$ , that is five periods of excitation. Note that there is no need for  $t_{\text{on/off}}$  here as  $V_b(t)$  slowly increase from zero in the beginning and vanishes at  $t = T_{\text{exc}}$ . We have found that for  $\omega_{\text{exc}}$  close to the Bogoliubov resonant frequency  $\omega_{\text{res}} = k_{\text{exc}} \sqrt{k_{\text{exc}}^2/4 + \mu_0}$ , large excitations could be created. For  $k_{\text{exc}} < 1/\xi$  we observe the creation of  $2M$  pairs of solitons:  $M$  clock-wise propagating degenerate solitons with the same velocity and  $M$  anti-clock-wise solitons with the opposite velocity, that are both initially created at the maxima of the potential. For  $k_{\text{exc}} > 1/\xi$  the modulation protocol results in a very regular state, with high periodicity, that also exhibits a complicated but periodic evolution in time, with no clear soliton propagation pattern. This corresponds to the state shown in Fig. 5, where  $M = 50$  and  $\omega_{\text{exc}} = 2.788\mu_0$  have been used. As explained in section IV this behavior can be recovered and understood using analytical methods by

considering an initial state of the form (4). This state can thus be created in an experiment either by shaping the initial state or by applying the realistic modulation protocol of Eq. (A2), starting from the groundstate.

## Appendix B: Computation of the Lax spectrum

The Lax eigenvalue equation we want to solve is  $\mathcal{L}v = \zeta v$ . In order to compute this equation in momentum space, we take the Fourier transform,  $\hat{\mathcal{L}} * \hat{v} = \zeta \hat{v}$ , where  $*$  is the convolution and  $\hat{v}$  is the Fourier transform of  $v$ . The equation then reads:

$$\begin{pmatrix} -\frac{k}{2}\hat{v}_1 - i\frac{\sqrt{g}}{2}\hat{\psi} * \hat{v}_2 \\ i\frac{\sqrt{g}}{2}\hat{\psi}^* * \hat{v}_1 + \frac{k}{2}\hat{v}_2 \end{pmatrix} = \zeta \begin{pmatrix} \hat{v}_1 \\ \hat{v}_2 \end{pmatrix}.$$

Now to compute the convolution, corresponding to off diagonal terms in  $\mathcal{L}$ , we have to write it using the discrete Fourier transform:  $\hat{\psi}(k) \rightarrow \hat{\psi}_q = \sum_{n=0}^{N_z-1} \psi_n e^{-ik_q x_n}$  where  $x_n$  or  $k_q$  belong to the discrete grid in position or momentum space. Then the discrete convolution reads:

$$[\hat{\psi} * \hat{v}]_q = \sum_{p=0}^{N_z-1} \hat{\psi}_{q-p} \hat{v}_p,$$

where the index  $q - p$  in the sum is taken modulo  $N_z$ , as  $\hat{\psi}_q = \hat{\psi}_{q+N_z}$ . This operation can be written in a matrix form:

$$C\hat{v} = \begin{pmatrix} \hat{\psi}_0 & \hat{\psi}_1 & \cdots & \hat{\psi}_{N_z-2} & \hat{\psi}_{N_z-1} \\ \hat{\psi}_{N_z-1} & \hat{\psi}_0 & \cdots & \hat{\psi}_{N_z-3} & \hat{\psi}_{N_z-2} \\ & & \cdots & & \\ \hat{\psi}_2 & \hat{\psi}_3 & \cdots & \hat{\psi}_0 & \hat{\psi}_1 \\ \hat{\psi}_1 & \hat{\psi}_2 & \cdots & \hat{\psi}_{N_z-1} & \hat{\psi}_0 \end{pmatrix} \hat{v}$$

from which it is clear that the convolution matrix has a Toeplitz structure.

Finally we diagonalize the  $2N_z \times 2N_z$  matrix:

$$L = \frac{i}{2} \begin{pmatrix} ik & -\sqrt{g}C \\ \sqrt{g}C^\dagger & -ik \end{pmatrix},$$

where  $k$  stands for the diagonal matrix of discrete wave-vectors. All operations are implemented in octave/matlab language using built-in functions.

## Appendix C: Collision between two solitons

The IST can be used to find analytical multiple dark soliton solutions for the 1DNLSE. When the solitons are well separated such solution is well approximated by a multiplication of two single soliton solution, see Eq. (3), with a proper normalization. We study here a collision between two solitons with angles  $\phi_1 = \pi/8$  and  $\phi_2 = \pi/4$ , corresponding to opposite velocities and resulting in a head-on collision, as shown in Fig. 8a). Using this two



soliton state, we calculate the Lax spectrum in which two isolated eigenvalues are present. For each eigenvalue we compute the associated  $\mathcal{M}$  value and, by finding the Lax spectrum at different times, we follow the evolution of the  $\mathcal{M}$  values during the collision, see Fig. 8b). As anticipated, during the collision the  $\mathcal{M}$  values decrease while remaining well above the phenomenological threshold  $\mathcal{M} > \mathcal{M}_c = 100$ . This may explain why the  $\mathcal{M}$  values are not distributed according to a simple law in Fig. 4b). We have checked that the same phenomenon occurs for various soliton angles.

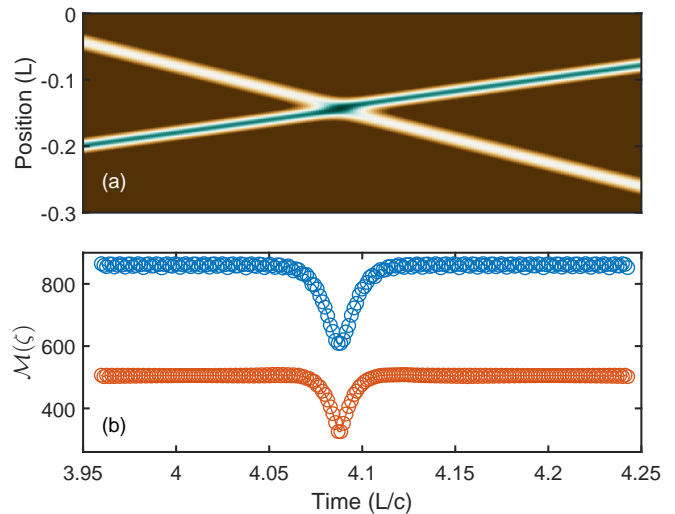


FIG. 8. (color online) a) Density map of a collision between two grey solitons with different velocity. b)  $\mathcal{M}$  value as a function of time for the isolated eigenvalues associated to the solitons. The  $\mathcal{M}$  values are smaller during the collision, while still remaining well above the phenomenological threshold  $\mathcal{M}_c = 100$ .

- 
- [1] S. A. Gredeskul and Y. S. Kivshar, Generation of dark solitons in optical fibers, *Physical Review Letters* **62**, 977 (1989).
  - [2] W. Zhao and E. Bourkoff, Propagation properties of dark solitons, *Opt. Lett.* **14**, 703 (1989).
  - [3] S. A. Gredeskul, Y. S. Kivshar, and M. V. Yanovskaya, Dark-pulse solitons in nonlinear-optical fibers, *Physical Review A* **41**, 3994 (1990).
  - [4] Y. Kivshar and S. Gredeskul, Dark solitons produced by phase steps in nonlinear optical fibers, *Optics Communications* **79**, 285 (1990).
  - [5] T. Bienaimé, M. Isoard, Q. Fontaine, A. Bramati, A. M. Kamchatnov, Q. Glorieux, and N. Pavloff, Quantitative analysis of shock wave dynamics in a fluid of light, *Physical Review Letters* **126**, 183901 (2021).
  - [6] M. Olshanii, Atomic scattering in the presence of an external confinement and a gas of impenetrable bosons, *Physical Review Letters* **81**, 938 (1998).
  - [7] S. Burger, K. Bongs, S. Dettmer, W. Ertmer, K. Sengstock, A. Sanpera, G. V. Shlyapnikov, and M. Lewenstein, Dark solitons in Bose-Einstein condensates, *Physical Review Letters* **83**, 5198 (1999).
  - [8] D. J. Frantzeskakis, Dark solitons in atomic Bose-Einstein condensates: from theory to experiments, *Journal of Physics A: Mathematical and Theoretical* **43**, 213001 (2010).
  - [9] A. Maître, F. Claude, G. Lerario, S. Koniakhin, S. Pigeon, D. Solnyshkov, G. Malpuech, Q. Glorieux, E. Giacobino, and A. Bramati, Spontaneous generation, enhanced propagation and optical imprinting of quantized vortices and dark solitons in a polariton superfluid: Towards the control of quantum turbulence, *EPL (Europhysics Letters)* **134**, 24004 (2021).
  - [10] P. Suret, A. Tikan, F. Bonnefoy, F. Copie, G. Ducrozet, A. Gelash, G. Prabhudesai, G. Michel, A. Cazaubiel, E. Falcon, G. El, and S. Randoux, Nonlinear spectral synthesis of soliton gas in deep-water surface gravity waves, *Physical Review Letters* **125**, 264101 (2020).
  - [11] V. E. Zakharov and A. B. Shabat, Interaction between solitons in a stable medium, *Zh. Eksp. Teor. Fiz* **64**, 1627 (1973).
  - [12] V. E. Zakharov and A. B. Shabat, A scheme for integrating the nonlinear equations of mathematical physics by the method of the inverse scattering problem. I, *Functional Analysis and Its Applications* **8**, 226 (1974).
  - [13] P. P. Kulish, S. V. Manakov, and L. D. Faddeev, Comparison of the exact quantum and quasiclassical results for a nonlinear Schrödinger equation, *Theoretical and Mathematical Physics* **28**, 615 (1976).
  - [14] M. J. Ablowitz and H. Segur, *Solitons and the Inverse Scattering Transform*, Vol. 127 (Society for Industrial and Applied Mathematics, 1981) p. 564.
  - [15] Y. S. Kivshar and B. A. Malomed, Dynamics of solitons in nearly integrable systems, *Rev. Mod. Phys.* **61**, 763 (1989).
  - [16] A. Gurevich and A. Krylov, Dissipationless shock waves in media with positive dispersion, *Zh. Eksp. Teor. Fiz* **92**, 1684 (1987).
  - [17] G. El and M. Hoefer, Dispersive shock waves and modulation theory, *Physica D: Nonlinear Phenomena* **333**, 11 (2016).
  - [18] Y. S. Kivshar and W. Królikowski, Instabilities of dark solitons, *Opt. Lett.* **20**, 1527 (1995).
  - [19] G. Theoharis, P. Schmelcher, M. K. Oberthaler, P. G. Kevrekidis, and D. J. Frantzeskakis, Lagrangian approach to the dynamics of dark matter-wave solitons,

- Physical Review A **72**, 023609 (2005).
- [20] C. H. Tenorio, E. V. Vargas, V. N. Serkin, M. A. Grana- dos, T. L. Belyaeva, R. P. Moreno, and L. M. Lara, Dy- namics of solitons in the model of nonlinear Schrödinger equation with an external harmonic potential: II. Dark solitons, *Quantum Electronics* **35**, 929 (2005).
  - [21] A. Muryshev, G. V. Shlyapnikov, W. Ertmer, K. Sen- gstock, and M. Lewenstein, Dynamics of dark solitons in elongated Bose-Einstein condensates, *Physical Review Letters* **89**, 110401 (2002).
  - [22] L. M. Aycok, H. M. Hurst, D. K. Efimkin, D. Genkina, H.-I. Lu, V. M. Galitski, and I. B. Spielman, Brownian motion of solitons in a Bose-Einstein condensate, *Proceedings of the Na- tional Academy of Sciences* **114**, 2503 (2017), <https://www.pnas.org/doi/pdf/10.1073/pnas.1615004114>.
  - [23] J. Denschlag, J. E. Simsarian, D. L. Feder, C. W. Clark, L. A. Collins, J. Cubizolles, L. Deng, E. W. Hagley, K. Helmerson, W. P. Reinhardt, S. L. Rolston, B. I. Schneider, and W. D. Phillips, Generating solitons by phase engineering of a Bose-Einstein condensate, *Science* **287**, 97 (2000).
  - [24] S. Stellmer, C. Becker, P. Soltan-Panahi, E.-M. Richter, S. Dörscher, M. Baumert, J. Kronjäger, K. Bongs, and K. Sengstock, Collisions of dark solitons in elongated Bose-Einstein condensates, *Physical Review Letters* **101**, 120406 (2008).
  - [25] L. D. Carr, J. Brand, S. Burger, and A. Sanpera, Dark- soliton creation in Bose-Einstein condensates, *Physical Review A* **63**, 051601(R) (2001).
  - [26] B. Wu, J. Liu, and Q. Niu, Controlled generation of dark solitons with phase imprinting, *Physical Review Letters* **88**, 034101 (2002).
  - [27] A. Romero-Ros, G. C. Katsimiga, P. G. Kevrekidis, B. Prinari, G. Biondini, and P. Schmelcher, On-demand generation of dark soliton trains in Bose-Einstein con- densates, *Physical Review A* **103**, 023329 (2021).
  - [28] V. Hakim, Nonlinear Schrödinger flow past an obstacle in one dimension, *Physical Review E* **55**, 2835 (1997).
  - [29] N. Bilas and N. Pavloff, Dark soliton past a finite-size obstacle, *Physical Review A* **72**, 033618 (2005).
  - [30] B. Jackson, N. P. Proukakis, and C. F. Barenghi, Dark- soliton dynamics in Bose-Einstein condensates at finite temperature, *Physical Review A* **75**, 051601(R) (2007).
  - [31] T. Karpiuk, P. Deuar, P. Bienias, E. Witkowska, K. Pawłowski, M. Gajda, K. Rzazewski, and M. Brewczyk, Spontaneous solitons in the thermal equilibrium of a quasi-1D Bose gas, *Physical Review Letters* **109**, 205302 (2012).
  - [32] M. Schmidt, S. Erne, B. Nowak, D. Sexty, and T. Gasen- zer, Non-thermal fixed points and solitons in a one- dimensional Bose gas, *New Journal of Physics* **14**, 075005 (2012).
  - [33] T. Karpiuk, T. Sowiński, M. Gajda, K. Rzazewski, and M. Brewczyk, Correspondence between dark solitons and the type II excitations of the Lieb-Liniger model, *Physical Review A* **91**, 013621 (2015).
  - [34] S. Guo, A. R. Fritsch, C. Greenberg, I. B. Spielman, and J. P. Zwolak, Machine-learning enhanced dark soliton de- tection in Bose-Einstein condensates, *Machine Learning: Science and Technology* **2**, 035020 (2021).
  - [35] B. Grébert and T. Kappeler, *The Defocusing NLS Equa- tion and Its Normal Form* (EMS Press, 2014) p. 166.
  - [36] L. D. Carr, C. W. Clark, and W. P. Reinhardt, Stationary solutions of the one-dimensional nonlinear Schrödinger equation. I. Case of repulsive nonlinearity, *Physical Re- view A* **62**, 063610 (2000).
  - [37] Y.-C. Ma and M. J. Ablowitz, The periodic cubic Schrödinger equation, *Studies in Applied Mathematics* **65**, 113 (1981).
  - [38] A. Osborne, Numerical inverse scattering transform for the periodic, defocusing nonlinear Schrödinger equation, *Physics Letters A* **176**, 75 (1993).
  - [39] A. Osborne, The hyperelliptic inverse scattering trans- form for the periodic, defocusing nonlinear Schrödinger equation, *Journal of Computational Physics* **109**, 93 (1993).
  - [40] T. Tsuzuki, Nonlinear waves in the Pitaevskii-Gross equation, *Journal of Low Temperature Physics* **4**, 441 (1971).
  - [41] V. A. Brazhnyi and A. M. Kamchatnov, Creation and evolution of trains of dark solitons in a trapped one- dimensional Bose-Einstein condensate, *Physical Review A* **68**, 043614 (2003).
  - [42] M. Tajik, B. Rauer, T. Schweigler, F. Cataldini, J. ao Sabino, F. S. Møller, S.-C. Ji, I. E. Mazets, and J. Schmiedmayer, Designing arbitrary one-dimensional potentials on an atom chip, *Opt. Express* **27**, 33474 (2019).
  - [43] P. B. Blakie, Numerical method for evolving the pro- jected Gross-Pitaevskii equation, *Physical Review E* **78**, 026704 (2008).
  - [44] A. K. Saha and R. Dubessy, Dynamical phase diagram of a one-dimensional Bose gas in a box with a tunable weak link: From Bose-Josephson oscillations to shock waves, *Physical Review A* **104**, 023316 (2021).
  - [45] M. Brachet, Gross-Pitaevskii description of superfluid dynamics at finite temperature: A short review of recent results, *Comptes Rendus Physique* **13**, 954 (2012).
  - [46] C. Raman, M. Köhl, R. Onofrio, D. S. Durfee, C. E. Kuk- lewicz, Z. Hadzibabic, and W. Ketterle, Evidence for a critical velocity in a Bose-Einstein condensed gas, *Phys- ical Review Letters* **83**, 2502 (1999).
  - [47] B. Damski, K. Sacha, and J. Zakrzewski, Stirring a Bose-Einstein condensate, *Journal of Physics B: Atomic, Molecular and Optical Physics* **35**, 4051 (2002).
  - [48] W. Weimer, K. Morgener, V. P. Singh, J. Siegl, K. Hueck, N. Luick, L. Mathey, and H. Moritz, Critical velocity in the BEC-BCS crossover, *Physical Review Letters* **114**, 095301 (2015).
  - [49] V. P. Singh, W. Weimer, K. Morgener, J. Siegl, K. Hueck, N. Luick, H. Moritz, and L. Mathey, Probing superfluid- ity of Bose-Einstein condensates via laser stirring, *Phys- ical Review A* **93**, 023634 (2016).
  - [50] H. Kiehn, V. P. Singh, and L. Mathey, Superfluidity of a laser-stirred Bose-Einstein condensate, *Physical Review A* **105**, 043317 (2022).